Eksakta : Berkala Ilmiah Bidang MIPA
VOLUME 27 NO 05 2026, pp 808-827
ISSN : Print 1411-3724 — Online 2549-7464
DOI : https://doi.org/10.24036/eksakta/vol27-iss05/733

Eksakta
Berkala Ilmiah Bidang MIPA
http://www.eksakta.ppj.unp.ac.id/index.php/eksakta

Article

Identification High Sulphidation Gold Mineralization Zones in the "R" Area Using the Induced Polarization Method

Article Info

Article history :
Received July 24, 2026
Revised August 25, 2026
Accepted September 03, 2026
Published October 30, 2026

Keywords :
High-sulfidation,
gold mineralization,
induced polarization,
resistivity, chargeability

Nisriinaa Nasywaa Ariefianty[1*], Yoqi Ali Taufan[2] , Budy Santoso[1]

[1]Department of Geophysics, Faculty of Mathematics and Natural Science, Universitas Padjadjaran, Bandung, Indonesia
[2]PT. Puncakbaru Jayatama, Jakarta, Indonesia

Abstract. Sumbawa Island, Indonesia, is part of the Sunda–Banda magmatic arc and has high potential for gold mineralization, particularly in high-sulfidation epithermal systems characterized by abundant sulfide minerals associated with highly acidic magmatic hydrothermal fluids. However, subsurface gold mineralization in Sumbawa Regency, West Nusa Tenggara Province, has not been specifically investigated. This study aims to identify subsurface gold mineralization zones using the Induced Polarization (IP) method, which is sensitive to sulfide minerals. Resistivity and chargeability data were integrated to characterize and delineate mineralization zones. Results show low resistivity values of 11.7–48.1 Ω·m associated with hydrothermal alteration and high chargeability values of 126–826.5 msec indicating disseminated sulfides. The anomalies occur within andesite host rock, show vertical continuity, and are associated with fault structures that provide pathways for hydrothermal fluid circulation. These structures are related to the Flores Back-Arc Thrust Belt and its splay faults. Integrated resistivity and chargeability anomalies indicate silicification zones or mineralized quartz veins containing disseminated sulfides as prospective gold mineralization targets. These results demonstrate that IP effectively identifies structurally controlled gold mineralization in high-sulfidation epithermal systems and improves exploration-zone delineation in Sumbawa Regency, thereby providing a basis for follow-up exploration programs and investigations in the area.

This is an open acces article under the CC-BY license.

This is an open access article distributed under the Creative Commons 4.0 Attribution License, which permits unrestricted use, distribution, and reproduction in any medium, provided the original work is properly cited. ©2026 by author.

Corresponding Author :
Nisriinaa Nasywaa Ariefianty
Department of Geophysics, Faculty of Mathematics and Natural Science, Universitas Padjadjaran, Bandung, Indonesia
Email : ririariefianty@gmail.com

1. Introduction

Indonesia has gold resources of approximately 3,420 metric tons (±114.3 million ounces), accounting for about 5% of global gold resources [1]. This potential is closely related to Indonesia's position at the convergence of the Eurasian, Indo-Australian, and Pacific tectonic plates, where intense subduction and magmatic activity have generated various hydrothermal systems and associated metallic deposits [2-3]. Gold deposits may occur as primary deposits formed by hydrothermal processes or as secondary placer deposits derived from the weathering and redistribution of pre-existing deposits [4-5]. Among primary deposits, epithermal systems are important exploration targets because they form from ascending hydrothermal fluids under relatively low-temperature and low-pressure conditions [6].

Sumbawa Island, located within the Sunda–Banda Arc, hosts diverse Au–Cu mineralization systems, including the high-sulfidation system at the Onto Prospect, low-sulfidation mineralization at Lamuntet, and Cu–Au porphyry systems at Batu Hijau and the Humpa Leu East (HLE) Prospect in Hu'u [7-10]. Recent studies at HLE have identified Cu–Au mineralization associated with intrusive rocks, hydrothermal alteration, quartz–sulfide veins, and disseminated sulfides such as pyrite and chalcopyrite [10]. These occurrences demonstrate that Sumbawa has favorable geological conditions for hydrothermal Au–Cu mineralization and remains prospective for further exploration.

Subsurface mineralization can be investigated using geophysical methods that respond to contrasts in the physical properties of rocks and mineralized zones. Among these methods, induced polarization (IP) is particularly useful for metallic mineral exploration because it is sensitive to polarizable minerals, especially disseminated sulfides such as pyrite [11]. Chargeability reflects the presence and distribution of polarizable materials, whereas resistivity provides complementary information on lithology, hydrothermal alteration, silicification, and geological structures [12-13]. However, the electrical response of mineralized zones can vary considerably depending on host-rock properties, alteration intensity, sulfide distribution, and mineralization style. Previous studies have reported high chargeability associated with both moderate resistivity (15–100 Ωm) in Cu–Au mineralization [13] and low resistivity (<200–250 Ωm) in gold-associated sulfide mineralization [14]. Similarly, sulfide mineralization in the Sangon-II low-sulfidation epithermal system was characterized by moderate resistivity (50–300 Ωm), high chargeability (>30 ms), and structural control by an N350°E-trending fault [15].

In contrast, other epithermal mineralization zones have been associated with high resistivity related to silicification or silica veins and elevated chargeability indicating sulfide-bearing zones [16-17]. In high-sulfidation systems, silica alteration commonly exhibits relatively high resistivity, whereas argillic alteration tends to produce lower resistivity and elevated chargeability; Au–Cu mineralization is generally associated with pronounced chargeability anomalies and structural or alteration-related contrasts in resistivity and magnetic properties [18-19]. These variations emphasize that IP anomalies must be interpreted within the local geological framework. These contrasting responses emphasize that IP anomalies should be interpreted within the local geological and alteration framework.

Despite the proven application of IP in gold exploration, information on the subsurface distribution of mineralization within Area R in Sumbawa Regency remains limited. Previous IP investigations on Sumbawa have been conducted in areas such as Plampang, but, based on the reviewed literature, no comparable study has specifically characterized the resistivity and chargeability distribution beneath Area R. Consequently, the geometry, depth, and vertical and lateral continuity

of potential mineralization zones in this area remain poorly constrained. These limitations highlight the need for further subsurface geophysical investigation to evaluate the mineralization potential of Area R.

Geologically (Figure 1), Area R is predominantly underlain by the Miocene Tuff-Breccia Unit (Tmv), consisting of andesitic volcanic breccia interbedded with tuff, tuffaceous sandstone, and other volcaniclastic deposits. The unit has undergone propylitic alteration, silicification, and mineralization, as indicated by quartz and calcite veins. Miocene intrusive rocks (Tmi), including andesite, basalt, and dacite, are also present and commonly contain pyrite, while Quaternary alluvial deposits (Qal) consist of unconsolidated gravel, sand, clay, and mud with locally magnetite-bearing sediments. These lithological, alteration, and sulfide characteristics indicate the development of a hydrothermal system favorable for gold mineralization.

The choice of geophysical method should therefore reflect the physical characteristics of the exploration target. Gravity and magnetic methods are useful for mapping density and magnetic-susceptibility contrasts related to lithology, intrusive bodies, and geological structures [20-21], while controlled-source audio-frequency magnetotellurics (CSAMT) can delineate resistivity variations, faults, intrusions, and hydrothermal fluid pathways. However, resistivity anomalies alone may be ambiguous because low resistivity can also result from clay, fluids, graphite, or structural zones [22]. In Area R, the occurrence of pyrite and other potentially disseminated sulfides makes IP particularly suitable because chargeability responds directly to polarizable sulfide minerals [12], while resistivity provides complementary constraints on alteration, silicification, lithological variations, and structural controls.

Therefore, this study integrates resistivity and chargeability data from IP measurements to identify and delineate potential sulfide-associated gold mineralization zones in Area R and evaluate their relationship with geological structures, thereby providing a basis for subsequent gold exploration activities in Sumbawa Regency.

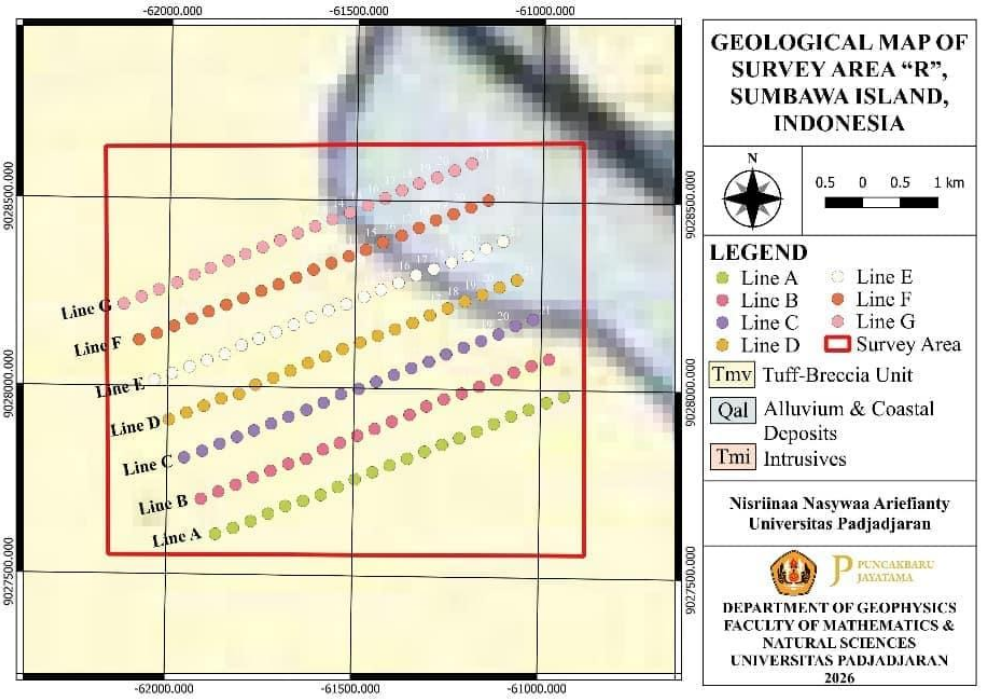


Figure 1. Regional geological map of the survey area

2. Method

2.1. Data Acquisition

Measurements were conducted in Sumbawa Regency, West Nusa Tenggara, Indonesia, along seven survey lines oriented from southwest to northeast (Figure 2), using a Zonge GDP-32 II instrument with a dipole–dipole configuration. Each line was 1 km long, with an electrode spacing of 50 m and a line spacing of 100 m, to determine the subsurface resistivity and chargeability distributions. Elevation was also measured at each electrode position using a total station.

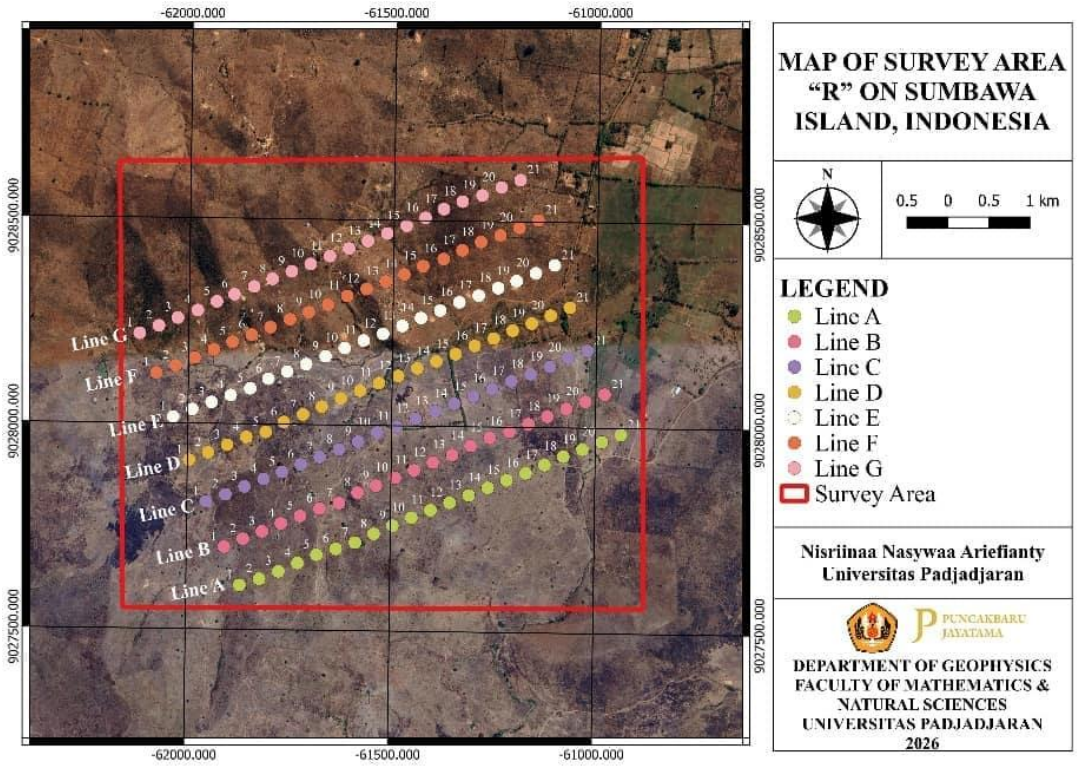


Figure 2. Map of the Induced Polarization Survey Area

2.2. Dipole –Dipole Array

The dipole–dipole configuration was chosen because it provides good horizontal resolution and sufficient depth of investigation, making it effective for mapping subsurface conditions. In this configuration, two current electrodes (C1–C2) and two potential electrodes (P1–P2) are used and positioned separately (Figure 3), so that allowing the distance between the two electrode pairs to be increased to obtain information from greater depths [23]. The geometric factor for the dipole–dipole configuration is defined as:

$$K = \pi n(n+1)(n+2)a \quad (1)$$

The measured resistivity data are then plotted based on the parameter n (n = 1, 2, 3, …), which represents the separation factor between the current and potential dipoles and is related to pseudo-depth. Using this approach, pseudo-depth cross-sections can be constructed to illustrate lateral and vertical variations in resistivity. The spacing between electrodes within each dipole is denoted by a, while the separation between the current and potential dipoles is expressed as na. As the value of n increases, the depth of investigation generally increases; however, the signal strength tends to decrease,

which may reduce data quality. In addition, measurement sensitivity is influenced by both the electrode spacing **a** and the separation factor n [24].

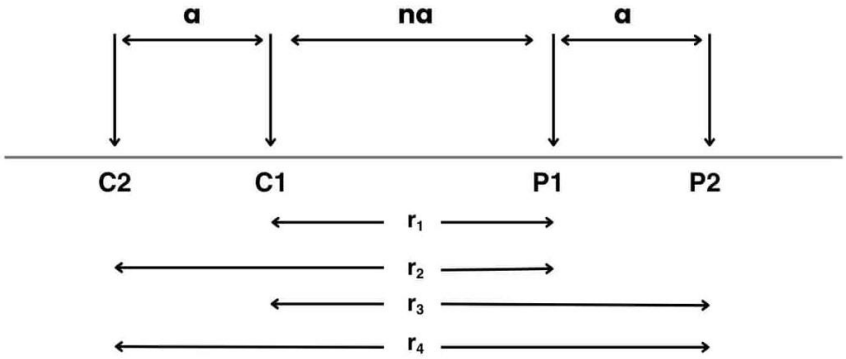


Figure 3. Electrode array of dipole-dipole

2.3. Data Processing

The measured apparent resistivity and chargeability data were inverted using RES2DINV to determine the distribution of subsurface electrical properties. Inversion is a mathematical and statistical procedure used to estimate subsurface models from observational data [25]. Topographic data obtained from a total station were incorporated by assigning the measured elevation to each electrode position along the survey lines and importing the elevation data together with the geoelectrical data. Subsurface discretization and forward modeling were performed using the Finite Element Method (FEM), whose mesh-based formulation represents irregular surface geometry and accounts for topographic variations during inversion [26]. The inversion employed an L2-norm smoothness-constrained least-squares approach because both the robust data and robust model constraints were disabled. A normal finite-element mesh with four nodes between adjacent electrodes, a model refinement factor of 0.5, and equal horizontal and vertical smoothing weights were applied [24].

The inversion used the logarithm of apparent resistivity and an initial damping factor of 0.15, which was automatically optimized to a minimum value of 0.02. The Jacobian matrix was calculated using the Gauss–Newton method, whereas model optimization employed the incomplete Gauss–Newton method. A maximum of seven iterations was specified, with a relative RMS-error change limit of 1.0% and an RMS convergence limit of 0.1%. The IP inversion was configured using the concurrent method with the separate inversion option rather than joint inversion, a damping factor of 0.25, and the same smoothness constraint as that applied to the resistivity model. A range transformation constrained the modeled chargeability values to 0–900 mV/V. The resulting 2D resistivity and chargeability models were evaluated based on the RMS misfit between the measured and calculated data.

The 2D inversion results were subsequently converted into XYZ format and integrated into a three-dimensional model in Oasis Montaj. Kriging interpolation was used to estimate the spatial distribution of resistivity and chargeability, whereas the results were visualized as vertical and horizontal slices using the minimum-curvature gridding method. Interpretation was based on established geophysical responses associated with mineralization. Mineralized zones are generally indicated by low-to-moderate resistivity and high chargeability, reflecting hydrothermal alteration and the presence of polarizable sulfide minerals [27]. Geological structures, particularly faults and fracture zones, were inferred from sharp lateral resistivity contrasts because these features may represent contrasts in rock properties as well as pathways for hydrothermal fluids [28].

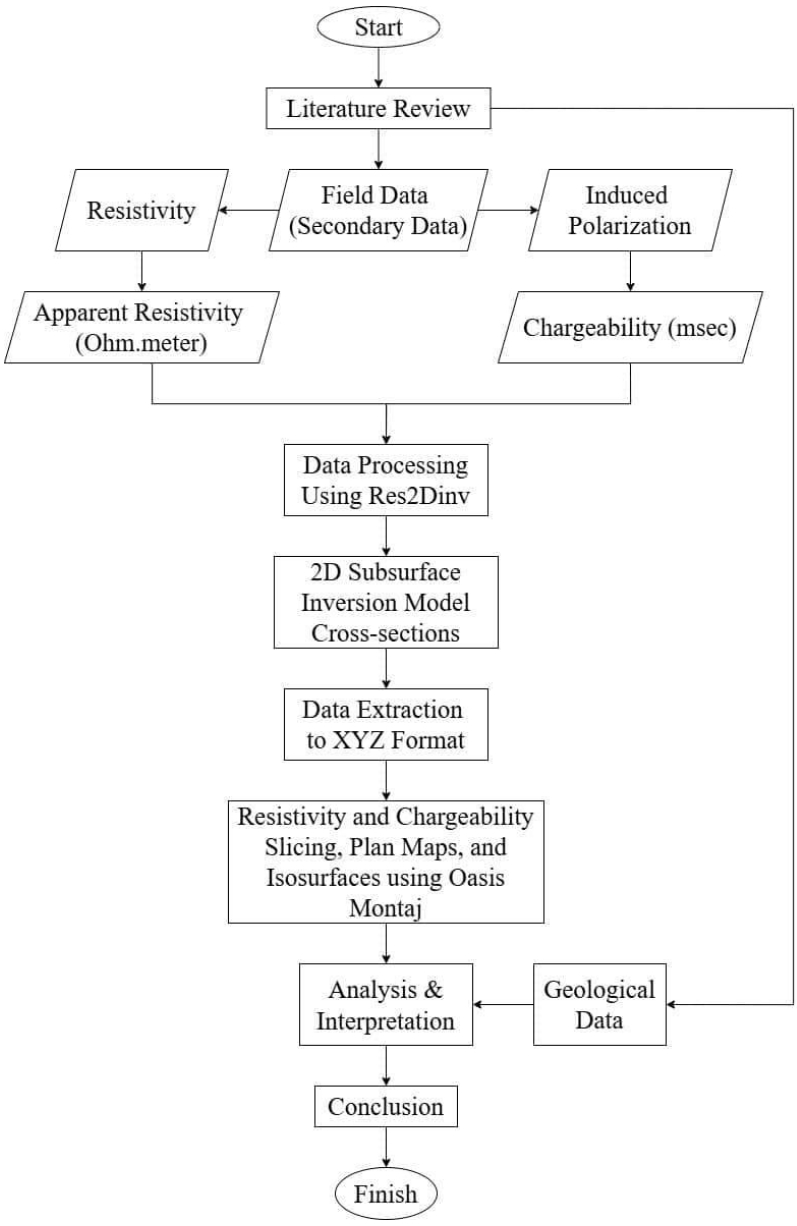


Figure 4. Flowchart of research

3. Results and Discussion

In this study, the IP method utilizes the chargeability properties that correlate with the content and distribution of sulfide minerals, making it effective for identifying subsurface mineralization zones associated with gold (Au) mineralization in high-sulfidation epithermal systems [29-30]. Interpretation of the mineralization zones is based on the correlation between resistivity and chargeability values obtained from data inversion results. Previous research has shown that hydrothermal gold mineralization is generally characterized by a combination of low resistivity and high chargeability associated with the presence of sulfide minerals. Previous studies indicate that hydrothermal gold mineralization is commonly associated with altered and fractured rocks, sulfide mineralization, and structurally controlled hydrothermal systems [31].

Table 1. Characteristics of Resistivity and Chargeability in Lithology, Alteration Zones, and Mineralization Zones

Lithology/Zone	Resistivity range (Ω·m)	Chargeability (msec)
Clay and sand	<100	<100
Tuff	>250	>100
Diorite and andesite (intrusions)	>500	>100
Argillic alteration zone	<100	>300
Silicic alteration zone	>100	>300
Gold mineralization/quartz vein zone	>250	>300
Propylitic alteration zone	<700	≥100

*Source: Adapted from Gautama, I. F. Y., Heditama, D. M., & Muttaqin, Y. A. (2018).

3.1 Interpretation of Induced Polarization

The integration of resistivity and chargeability cross-sections along the entire survey line reveals a consistent pattern of anomalies indicating the presence of a high-sulfidation epithermal gold mineralization system. Prospect zones are generally characterized by an association of low resistivity (11.7–48.1 Ω·m) and high chargeability (126–826.5 msec). The low-resistivity response is interpreted to reflect hydrothermally altered rocks, whereas the elevated chargeability indicates the presence of polarizable minerals, particularly disseminated sulfides. Therefore, the spatial coincidence of these two parameters provides the principal geophysical criterion for delineating prospective mineralization zones in the study area. A comparable relationship was reported in a Cu–Au mineralized system [13], where moderate resistivity (15–100 Ω·m) and high chargeability (>25 mV/V) were associated with disseminated pyrite and chalcopyrite. Although the geological setting differs from that of the present study, the comparable resistivity–chargeability relationship supports the interpretation that the identified anomalies represent sulfide-bearing hydrothermal zones. Their association with potential gold mineralization is further constrained by the geological, alteration, and structural characteristics of the study area.

The low resistivity values are interpreted as representing andesitic rocks affected by hydrothermal alteration, where increased conductivity may result from alteration products and conductive minerals. Previous studies have shown that high-sulfidation systems affected by argillic alteration commonly exhibit resistivity values below 50 Ω·m [19]. A comparable low-resistivity response (<200–250 Ω·m) associated with elevated chargeability has also been reported in another gold-mineralized system [14]. Although the absolute resistivity values differ from those obtained in the present study, the similar electrical response supports the interpretation of the anomalies as hydrothermally altered, sulfide-bearing zones. Electrical conductivity in such zones may be enhanced by interconnected sulfide minerals, including pyrite and chalcopyrite [32]. Consequently, low resistivity in the study area is interpreted primarily as a response to hydrothermal alteration and associated conductive minerals rather than as a direct indicator of gold.

High chargeability anomalies are interpreted as reflecting polarizable minerals, particularly disseminated sulfides. The observed values of 126–826.5 msec indicate strong polarization responses consistent with sulfide-bearing mineralized zones. In the Maletoyvaemskoie Ore Field, which hosts several high-sulfidation gold deposits, most identified ore bodies were characterized by elevated chargeability [33]. Although high chargeability is not uniquely diagnostic of gold mineralization, the occurrence of similarly elevated chargeability in another high-sulfidation system supports the interpretation that the anomalies identified in the present study represent prospective sulfide-bearing zones.

Profiles A, B, C, F, and G (Figures 5–7 and 10–11) show a relatively consistent association between low resistivity and high chargeability, without clear evidence of dominant fault-related discontinuities in the cross-sections. In Profile A, a prospective zone occurs at approximately 600 m along the line and at a depth of about 50 m in the northeastern part of the profile, with chargeability values of 126–342.3 msec. Profile B shows a similar anomaly at approximately 250 m along the line and at a depth of about 90 m in the southwestern part, with the same chargeability range. In Profile C, several prospective zones occur at approximately 200–400 m, 500 m, and 600 m along the line, generally extending to depths of about 50 m and exhibiting higher chargeability values of 126–826 msec. These broader and stronger anomalies suggest a more extensive distribution of sulfide-bearing alteration. Profiles F and G also contain prospective zones at approximately 300 m and 300–400 m along the lines, respectively, at depths of about 60 m and 40 m, with chargeability values reaching 826.5 msec. Overall, although the magnitude and spatial extent of the anomalies vary among the profiles, their consistent low-resistivity–high-chargeability association suggests differences in the concentration and distribution of sulfide minerals within the hydrothermal system.

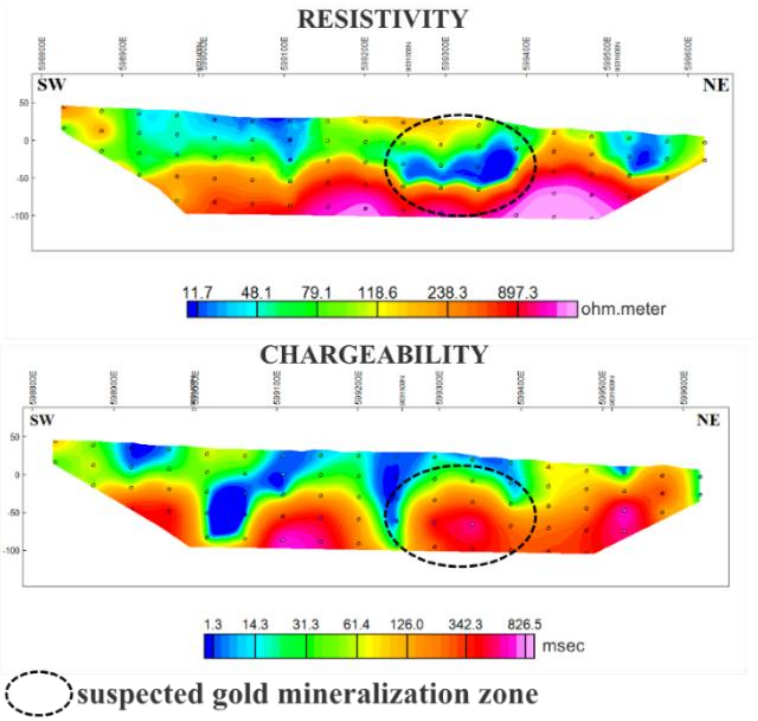


Figure 5. Profile of Line A

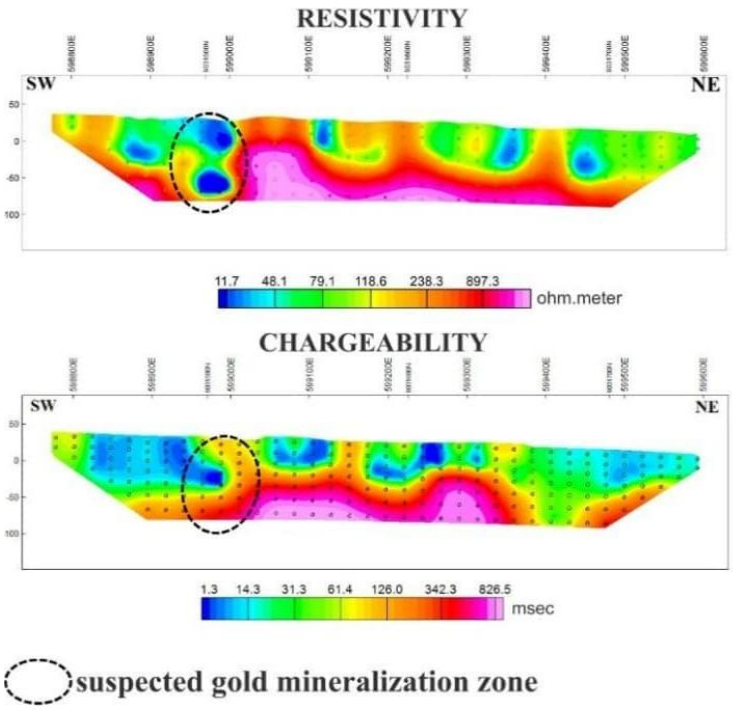


Figure 6. Profile of Line B

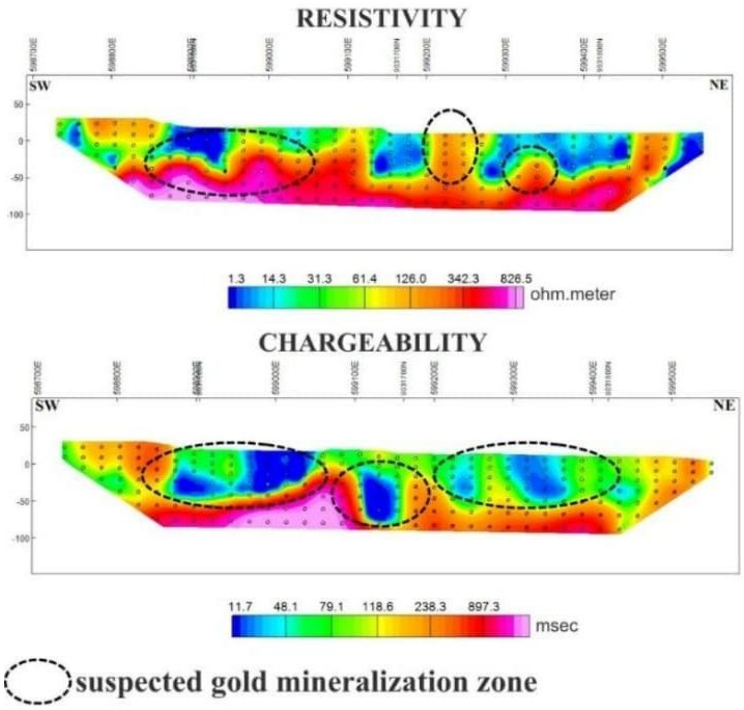


Figure 7. Profile of Line C

In contrast to Profiles A, B, C, F, and G, Profiles D and E (Figures 8–9) show prospective low-resistivity and high-chargeability anomalies associated with sharp lateral resistivity contrasts and discontinuities interpreted as fault or fracture zones. These weak zones may serve as pathways for hydrothermal-fluid migration [34]. Along Profile D, the prospective zone extends over a distance of approximately 400–600 m at a depth of about 50 m and has chargeability values of 182.7–521.7 msec. Along Profile E, the prospective zone is located at a distance of approximately 600–700 m at a depth of about 60 m and has chargeability values of 126–342.3 msec. The presence of fault structures is believed to control hydrothermal fluid circulation, thereby enhancing the accumulation of sulfide minerals and playing a role in the alteration and deposition of gold mineralization.

A comparable relationship between structural features and IP anomalies was reported at the Sarakan Gold Deposit, where high-polarization anomalies spatially coincided with known orebodies and fault-alteration zones. The integrated interpretation indicated that faults served as pathways for hydrothermal fluids and favorable sites for mineralization, particularly near fault intersections [35]. Although the Sarakan deposit represents a structurally controlled quartz–pyrite vein-type system rather than a high-sulfidation epithermal system, these findings support the interpretation that the structural features observed along Profiles D and E may have facilitated hydrothermal-fluid migration and localized sulfide deposition.

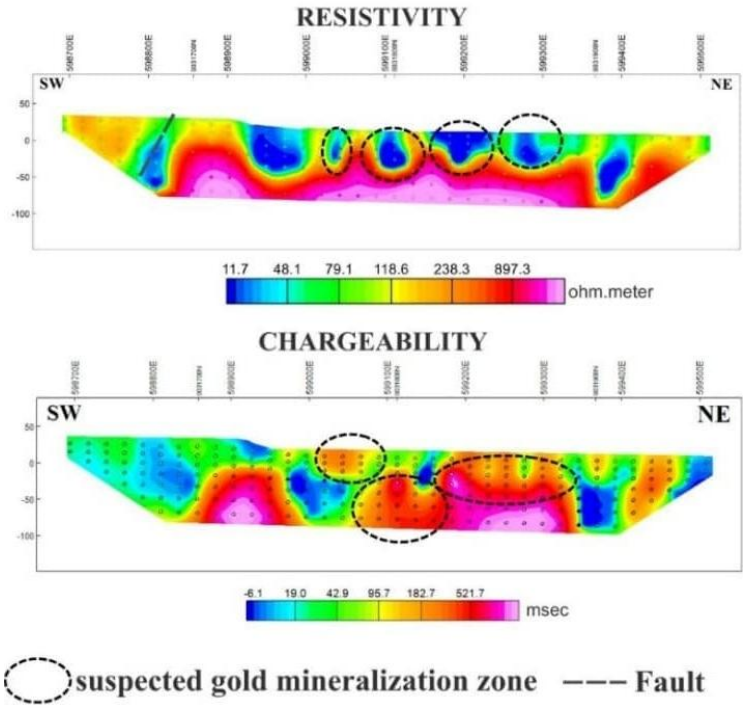


Figure 8. Profile of Line D

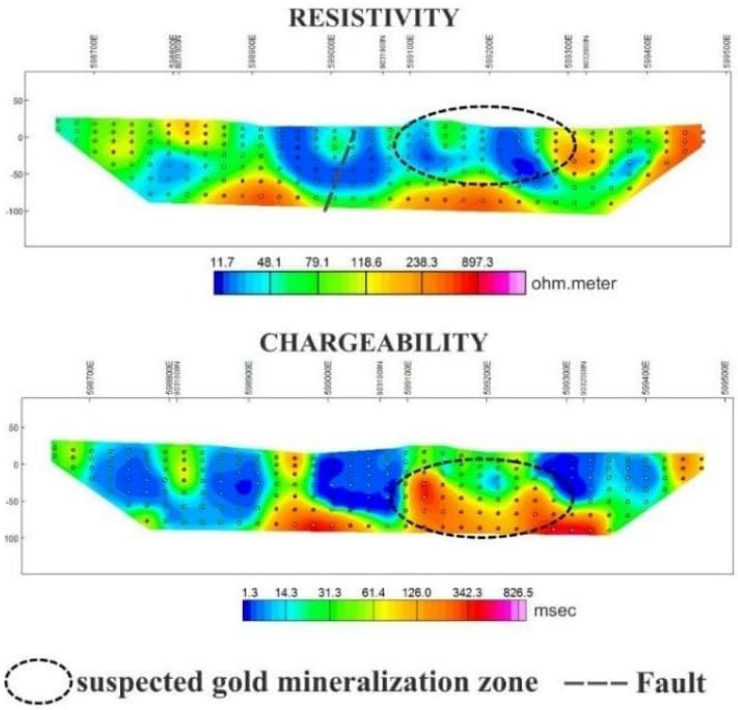


Figure 9. Profile of Line E

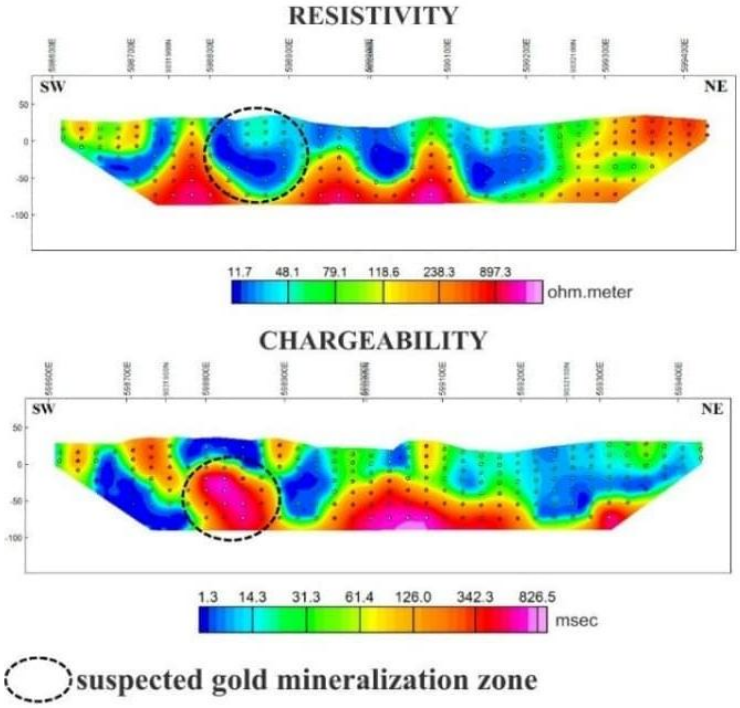


Figure 10. Profile of Line F

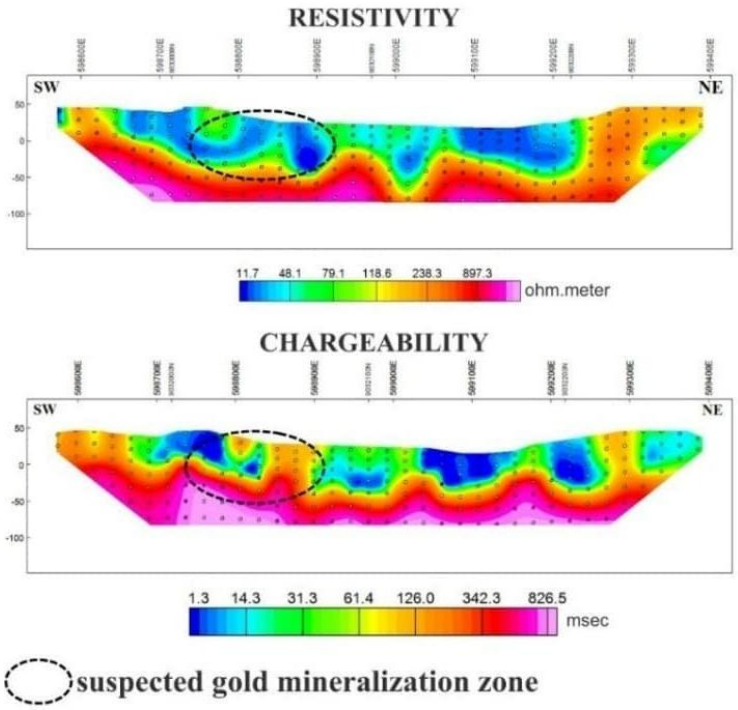


Figure 11. Profile of Line G

Overall, the seven profiles demonstrate a spatial relationship between low resistivity and high chargeability that is consistent with hydrothermal alteration containing disseminated sulfide minerals. Variations in chargeability magnitude and anomaly geometry likely reflect differences in sulfide concentration, distribution, alteration intensity, and local lithological conditions. Profiles D and E additionally indicate structural control, suggesting that faults and fractures may have enhanced hydrothermal-fluid circulation and localized mineralization.

In contrast to the predominantly low-resistivity and high-chargeability response observed in the present study, prospective gold mineralization characterized by high resistivity and high chargeability has also been reported, where the response was interpreted to reflect disseminated sulfides associated with a quartz-rich mineralized zone [36]. This contrasting response indicates that resistivity alone does not provide a unique signature of gold mineralization because it is strongly influenced by lithology, silicification, alteration, fracturing, fluid content, and sulfide distribution. Nevertheless, elevated chargeability remains an important indicator of polarizable sulfide minerals. Therefore, prospective zones in the present study are interpreted using the integrated relationship between resistivity, chargeability, and geological structures rather than a single geophysical parameter.

3.2 Identification of Structures Based on Isoresistivity Maps

Isoresistivity maps constructed at elevations from +50 m RL to −100 m RL reveal systematic changes in resistivity distribution with depth and provide information on the vertical development of the subsurface hydrothermal and structural system. Reduced Level (RL) represents the elevation of a point relative to an adopted vertical datum [37]. At shallow elevations from +50 m RL to +20 m RL, low- to moderate-resistivity zones ranging from approximately 118 to 1,053 Ωm dominate the central part of the survey area and are spatially associated with several mapped structural trends. These anomalies form elongated patterns that broadly follow the interpreted structures and are therefore considered to represent fractured, altered, and/or fluid-rich rock zones. Low-to-moderate resistivity values in

hydrothermal gold mineralization systems are generally associated with alteration processes, increased clay mineral content, and the presence of disseminated sulfide minerals that enhance rock conductivity [36].

A comparable relationship between electrical anomalies, alteration, and structural control was reported in the Sanjiaoding gold district, China. The IP survey showed that the electrical response of mineralized zones was strongly influenced by host-rock composition, alteration, fracturing, and sulfide content. Limonitized basalt exhibited low resistivity and high polarization, whereas pyrite-bearing monzogranite and gabbro were characterized by high resistivity and high polarization. Brittle fractures and ductile shear zones also controlled the orientation and distribution of mineralized bodies by providing pathways for hydrothermal-fluid migration [38]. These contrasting electrical responses indicate that structurally controlled gold mineralization does not exhibit a unique resistivity signature. Accordingly, the elongated low- to moderate-resistivity anomalies identified at shallow elevations in the present study are interpreted as fractured and altered zones potentially associated with structural pathways, while their mineralization potential is evaluated together with chargeability and geological evidence.

The orientation of these anomalies broadly corresponds with regional structural trends associated with the Flores Back-Arc Thrust Belt, which developed in response to regional shortening related to convergence between the Indo-Australian and Sunda plates [39-43]. Regional structural studies further indicate the development of a complex system of splay faults rooted in a deeper decollement surface at approximately 13–15 km depth [44]. These regional tectonic characteristics support the interpretation that the structural patterns observed in the isoresistivity maps may represent fault- and fracture-related zones associated with the broader Flores Back-Arc tectonic system. Such structures may enhance rock permeability and provide favorable pathways for hydrothermal-fluid migration and mineral deposition.

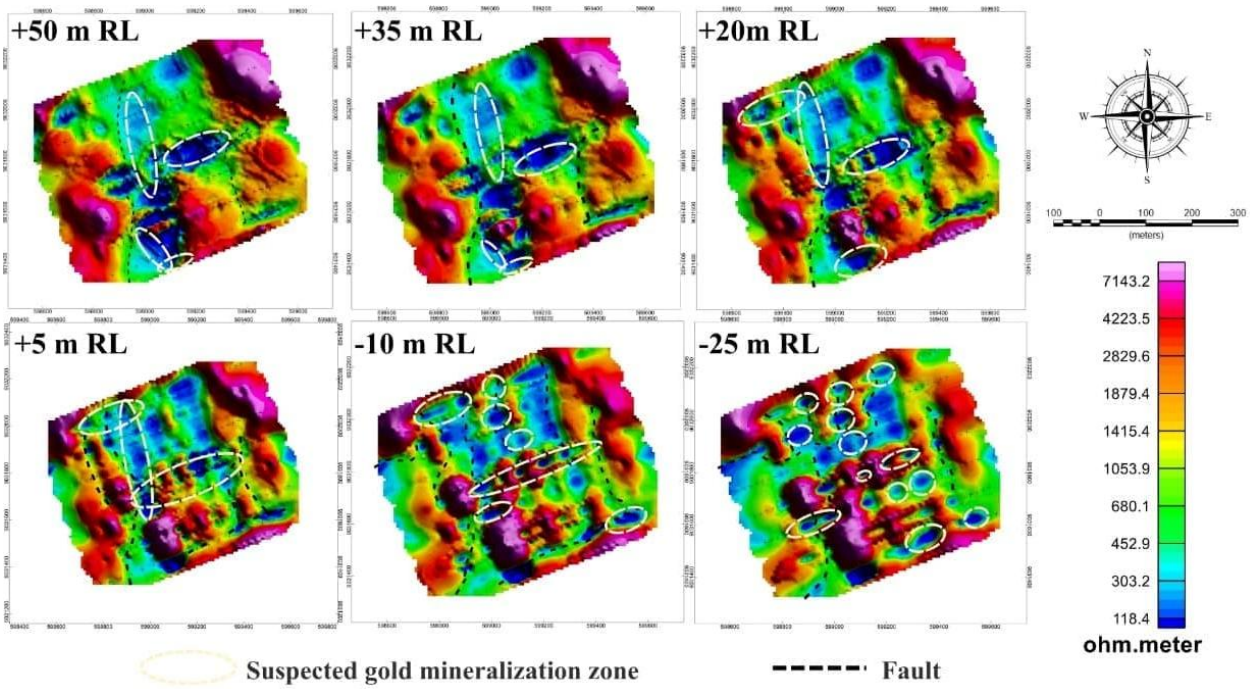


Figure 12. Iso-Resistivity Map from +50 m RL to -25 m RL

At intermediate elevations from +5 m RL to -25 m RL, the anomalies become more numerous and spatially extensive than those observed at shallower levels. Most remain concentrated along the main structural trends and develop elongated, lens-shaped, or elliptical geometries. Their spatial alignment suggests that geological structures exert an important control on hydrothermal-fluid migration. The presence of moderate resistivity anomalies in this zone may represent transitional zones between altered host rock and more silicified or quartz-rich zones. Gold mineralization is often associated with fault and fracture structures within hydrothermal systems. Mineralizing fluids move through permeable zones controlled by geological structures, subsequently depositing economically viable minerals at locations with increased porosity and permeability [36].

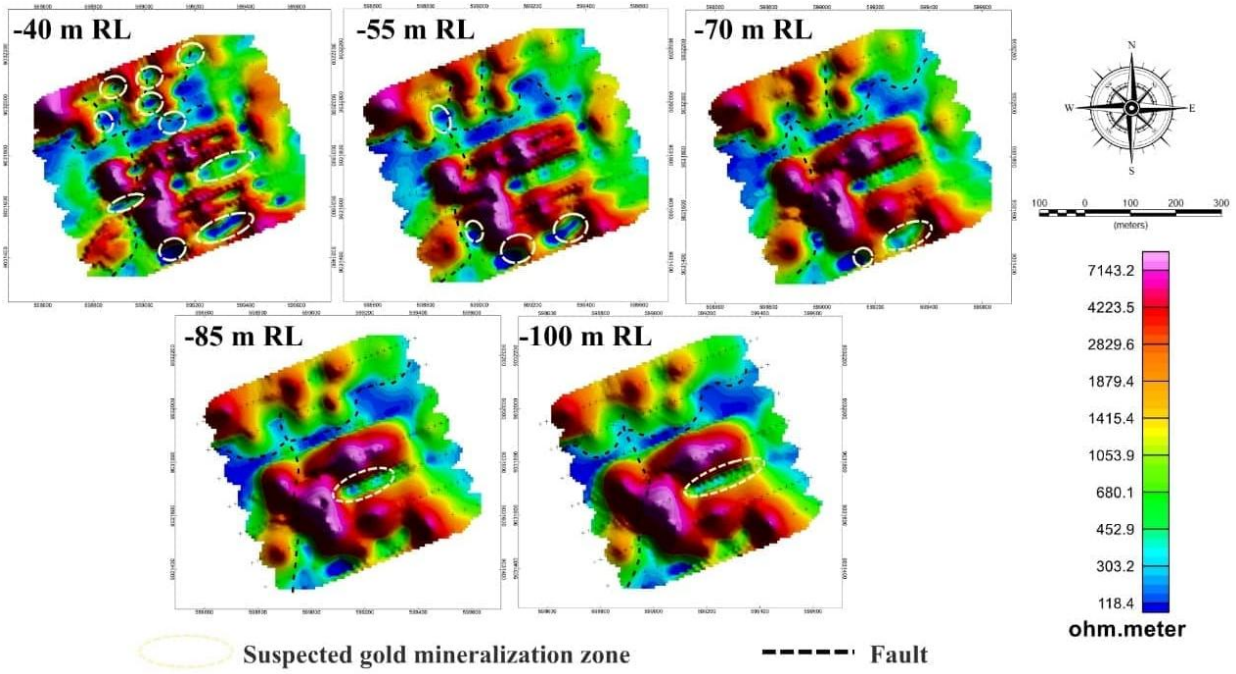


Figure 13. Iso-Resistivity Map -40 m RL to -100 m RL

At greater depths, particularly between −40 m RL and −55 m RL, the resistivity pattern changes markedly as a high-resistivity zone becomes increasingly dominant in the central part of the survey area. This zone reaches values exceeding 4,000 Ω·m and is more spatially concentrated than the anomalies observed at shallower elevations. Its geometry, high resistivity, and continuity along the structural trend suggest the development of an intensely silicified or quartz-rich hydrothermal zone. Relatively high resistivity responses have been associated with silicified zones [13], while mineralized rocks may exhibit either low- or high-resistivity responses depending on host-rock properties, alteration, and sulfide distribution [38]. Therefore, the high-resistivity anomaly identified in the present study is interpreted as a possible silicified or quartz-rich hydrothermal zone rather than as a direct indicator of gold mineralization. Its spatial continuity along the interpreted structural trend further suggests that this zone may represent a favorable pathway or site for hydrothermal-fluid migration and mineral deposition [45].

At elevations from -70 m RL to -100 m RL, the anomaly distribution becomes increasingly focused, with one major elongated anomaly remaining parallel to the interpreted structural trend. This feature exhibits vertical continuity from approximately −40 m RL to −100 m RL, suggesting the persistence of a structurally controlled hydrothermal zone at depth. Similar structurally controlled

mineralization has been reported in the El Bagre district, where elongated ore shoots were associated with fault and shear structures that enhanced permeability and mineralizing-fluid flow [46]. A comparable structural relationship is observed in the present study, where the deep resistivity anomaly exhibits an elongated geometry, vertical continuity, and spatial alignment with the interpreted fault trend, suggesting that the structure may have provided a persistent pathway for hydrothermal-fluid migration and localized mineral deposition. However, the El Bagre interpretation was constrained by structural and gold-grade data from drilling and channel samples [47], whereas the present study relies solely on geophysical evidence. Therefore, the anomaly is interpreted as a prospective structurally controlled mineralization zone rather than a confirmed ore shoot.

3.3 Identification of Gold Mineralization Based on Isochargeability

The geophysical interpretation presented in this study is inherently ambiguous because similar resistivity and chargeability responses may be produced by different combinations of lithology, hydrothermal alteration, sulfide minerals, fractures, and fluid content. Therefore, high chargeability anomalies cannot be interpreted as direct evidence of gold mineralization, but rather as indications of polarizable sulfide-bearing zones that may be associated with mineralization. Since this study relies solely on IP data, further validation using drilling, geochemical sampling, petrographic analysis, and mineragraphic examination is required to confirm the mineralogical composition and gold content of the interpreted anomalies.

The iso-chargeability map at elevations from +50 m RL to −100 m RL shows chargeability values chargeability values ranging from approximately 23.8 to 890.6 msec. High-chargeability anomalies are generally distributed along the same structural trends identified in the isoresistivity maps, indicating that the distribution of polarizable minerals is closely related to the subsurface structural framework. These anomalies are interpreted to reflect concentrations of disseminated sulfide minerals, potentially including pyrite, chalcopyrite, and arsenopyrite, within hydrothermally altered zones. The IP method is known to be highly sensitive to the presence of disseminated sulfide minerals. Therefore, the spatial relationship between elevated chargeability, resistivity variations, and geological structures provides an important basis for identifying prospective mineralized zones [36].

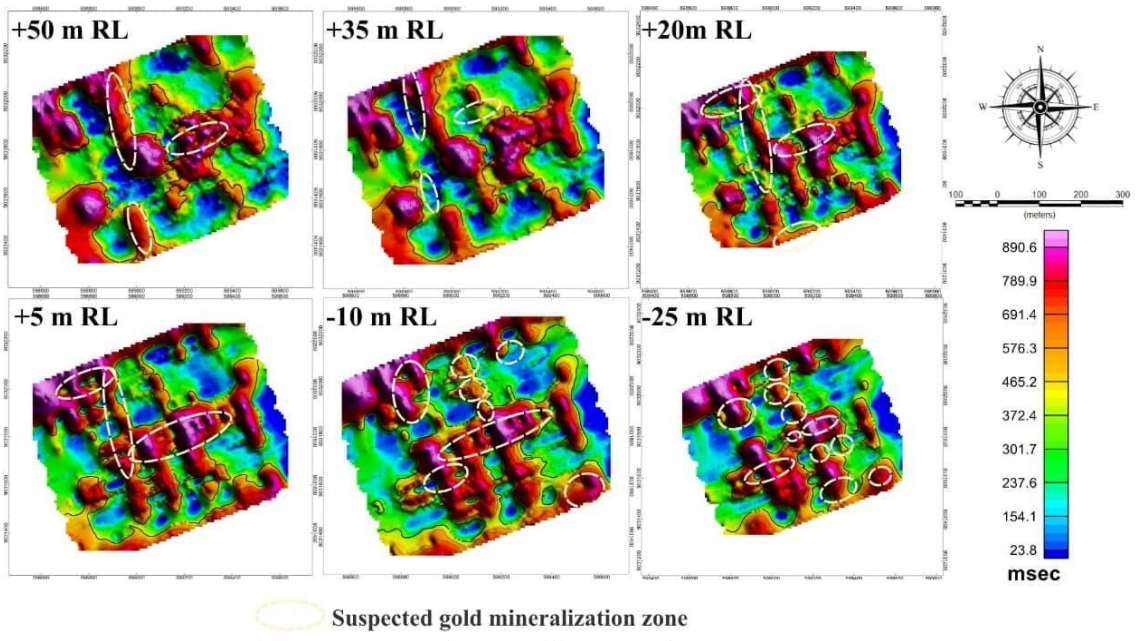


Figure 14. Iso-Chargeability Map from +50 m RL to -25 m RL

At shallow elevations from +50 m RL to +20 m RL, high chargeability anomalies are concentrated in the central to eastern parts of the survey area and are associated with previously mapped fault structures. Comparison with the corresponding isoresistivity maps shows that these anomalies are generally associated with low- to moderate-resistivity zones. This combination is interpreted as hydrothermally altered and fractured rock containing disseminated sulfides rather than massive quartz-dominated zones. Comparable associations between elevated chargeability, resistivity anomalies, and structural control have been reported in Cu–Au and low-sulfidation epithermal mineralization systems [13-15]. Although these studies represent different geological settings, they support the interpretation of the anomalies in Area R as sulfide-bearing hydrothermal zones rather than direct indicators of gold mineralization. In the present study, the chargeability range of 126–826.5 msec and its association with low- to moderate-resistivity anomalies and structural trends therefore strengthen the interpretation of these zones as prospective targets.

At elevations from +5 m RL to -25 m RL, high-chargeability anomalies become more extensive, forming elongated patterns parallel to the main structural trends. These anomalies increasingly coincide with moderate- to high-resistivity zones interpreted from the isoresistivity maps as silicified rocks or quartz-rich zones. The spatial coincidence of elevated chargeability and increased resistivity may reflect the coexistence of silicified or quartz-rich rocks and disseminated sulfide minerals within the same hydrothermal system. Relatively high resistivity responses have been associated with silicified zones, whereas elevated chargeability has been linked to polarizable sulfide minerals [13]. However, sulfide-bearing mineralized rocks may exhibit contrasting resistivity responses depending on lithology, alteration, and sulfide distribution [38]. Therefore, the combined high-resistivity and high-chargeability response observed in the present study is interpreted as a prospective silicified and sulfide-bearing zone, rather than as direct evidence of gold mineralization. Consequently, the integration of both parameters provides a more reliable basis for delineating prospective mineralized zones than interpretation of either resistivity or chargeability alone.

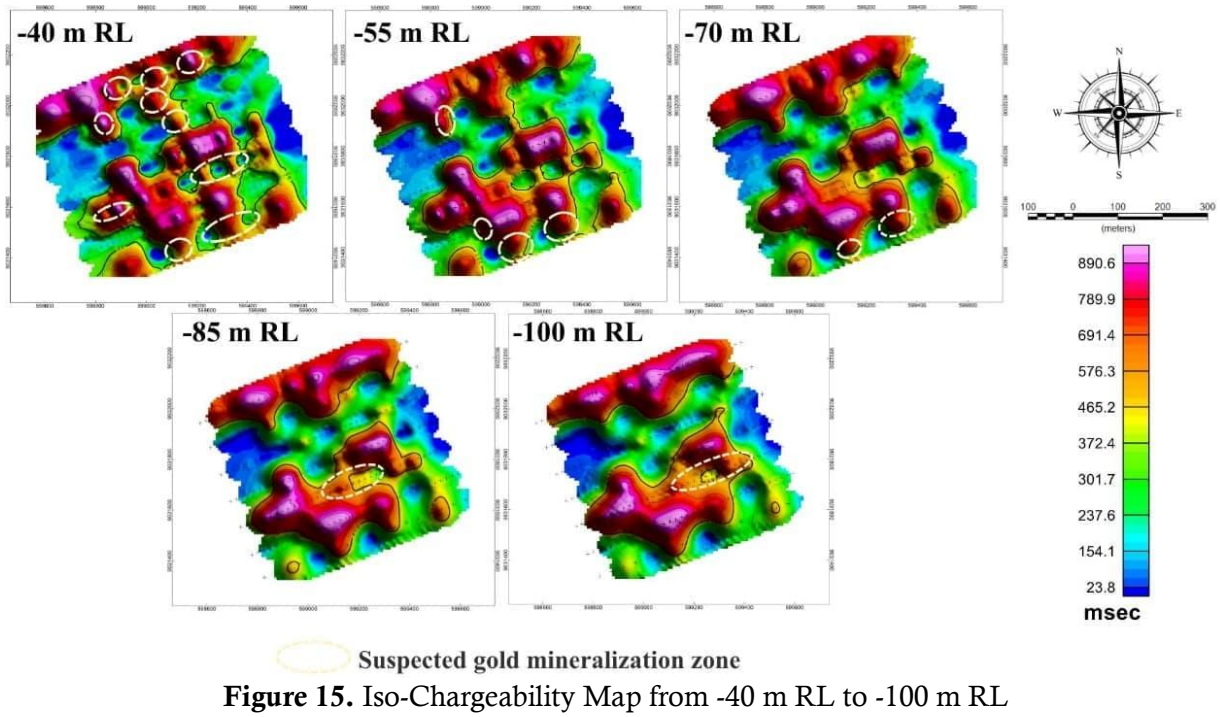


Figure 15. Iso-Chargeability Map from -40 m RL to -100 m RL

At elevations between −40 m RL and −70 m RL, the high-chargeability anomalies become more focused and show stronger spatial coincidence with the high-resistivity zones identified in the isoresistivity maps. This spatial relationship is interpreted as indicating a silicified hydrothermal zone containing polarizable sulfide minerals, where the resistivity response may be influenced by silicification and host-rock properties, while elevated chargeability primarily reflects the presence of disseminated sulfides. However, because these electrical responses are non-unique, the anomaly is interpreted as a prospective mineralized zone rather than a confirmed gold-bearing zone. At deeper elevations from −85 m RL to −100 m RL, only one dominant elongated chargeability anomaly remains. This feature coincides spatially with the vertically continuous resistivity anomaly observed between approximately −40 m RL and −100 m RL and follows the interpreted structural trend. The persistent association of elevated chargeability with moderate- to high-resistivity values therefore suggests a silicified, sulfide-bearing zone or mineralized quartz-vein system developed along a major hydrothermal pathway. Among the anomalies identified in the study area, this vertically continuous resistivity–chargeability feature represents the most prospective target for further gold exploration.

Although the identified anomalies cannot be considered confirmed gold-bearing zones due to the non-unique nature of geophysical responses, their consistent resistivity–chargeability association, vertical continuity, and spatial relationship with geological structures provide a strong basis for prioritizing these zones for subsequent exploration. Further validation through drilling, geochemical sampling, petrographic analysis, and mineragraphic examination is required to confirm the mineralogical composition and gold content of the interpreted anomalies.

4. Conclusion

The integration of resistivity and chargeability data successfully delineated prospective sulfide-associated mineralization zones in Area R. In the 2D profiles, the main prospective zones are characterized by low resistivity values of 11.7–48.1 Ω·m and high chargeability values of 126–826.5 msec, interpreted as hydrothermally altered andesitic rocks containing disseminated sulfide minerals. Several anomalies are also spatially associated with fault and fracture zones that may have acted as pathways for hydrothermal-fluid circulation.

Isoresistivity and isochargeability maps from +50 m RL to −100 m RL show systematic changes with depth. At shallow elevations, high chargeability is mainly associated with low- to moderate-resistivity zones, whereas at greater depths it increasingly coincides with moderate- to high-resistivity anomalies interpreted as silicified or quartz-rich zones containing polarizable sulfides. At approximately −85 m RL to −100 m RL, one dominant elongated chargeability anomaly coincides with a vertically continuous resistivity anomaly extending from about −40 m RL to −100 m RL. Its continuity and alignment with the interpreted structural trend make this zone the principal target for further gold exploration.

Overall, the integration of resistivity, chargeability, and structural information provides a useful basis for delineating prospective mineralized zones in the high-sulfidation epithermal system. However, these anomalies should not be considered confirmed gold-bearing zones because geophysical responses are non-unique. Further validation through drilling, geochemical sampling, petrographic analysis, and mineragraphic examination is therefore required.

References

[1] Kementerian Energi dan Sumber Daya Mineral (ESDM). (2026). Evaluasi Kebijakan Bea Keluar Emas: Menjaga Hilirisasi, Menghindari Distorsi Pasar. Retrieved From Direktorat Jenderal Minerba, https://www.minerba.esdm.go.id/berita/minerba/detil/20260316-evaluasi-kebijakan-bea-keluar-emas-menjaga-hilirisasi-menghindari-distorsi-pasar. Accessed April 15, 2026.

[2] Hall, R. (2002). Cenozoic geological and plate tectonic evolution of SE Asia and the SW Pacific: computer-based reconstructions, model and animations. *Journal of Asian Earth Sciences*, *20*(4), 353–431.
[3] Hall, R. (2009). The Eurasian SE Asian margin as a modern example of an accretionary orogen. *Geological Society Special Publication*, *318*.
[4] Melchiorre, E. B., Mathur, R., Kamenov, G., & Paredes, J. (2023). Geochemical Overprinting and Secondary Placer Crystal Formation in the La Cholla District, Quartzsite, Arizona, USA: Evidence from Copper Isotopes, Morphology, and Trace Elements. *Minerals, 13(11), 1444*.
[5] dos Santos Alves, K., Sánchez, S. B., Barreiro, J. G., Palomares, R. M., & Prieto, J. M. C. (2020). Morphological and compositional analysis of alluvial gold: The Fresnedoso gold placer (Spain). *Ore Geology Reviews*, *121*, 103489.
[6] Hedenquist, J. W., Arribas, A., & Gonzalez-Urien, E. (2000). Chapter 7 Exploration for Epithermal Gold Deposits. In *SEG Reviews* (Vol. 13).
[7] Burrows, D. R., Rennison, M., Burt, D., & Davies, R. (2020). The Onto Cu-Au discovery, eastern Sumbawa, Indonesia: A large, middle Pleistocene lithocap-hosted high-sulfidation covellite-pyrite porphyry deposit. *Economic Geology*, *115*(7), 1385-1412.
[8] Ernawati, R., Idrus, A., & Petrus, H. T. B. M. (2019). Mineralogy and Geochemistry of Gold Ore Low Sulfidation -Epithermal at Lamuntet, Brang Rea, West Sumbawa District, West Nusa Tenggara Province. *Journal of Geoscience, Engineering, Environment, and Technology*, *4*(3), 198.
[9] Schirra, M., Laurent, O., Zwyer, T., Driesner, T., & Heinrich, C. A. (2022). Fluid Evolution at the Batu Hijau Porphyry Cu-Au Deposit, Indonesia: Hypogene Sulfide Precipitation from a Single-Phase Aqueous Magmatic Fluid During Chlorite–White-Mica Alteration. *Economic Geology*, *117(5),* 979-1012.
[10] Fadlin, Takahashi, R., Agangi, A., Sato, H., Idrus, A., Sutopo, B., & Pratiwinda, R. (2023). Geology, mineralization and calcite-rich potassic alteration at the Humpa Leu East (HLE) porphyry Cu-Au prospect, Hu'u district, Sumbawa Island, Indonesia. *Resource Geology*, *73*(1), e12309.
[11] Telford, W.M., Geldart, L.P. and Sheriff, R.E. (1990) Applied Geophysics. 2nd Edition, Cambridge University Press, Cambridge, 770.
[12] Revil, A., Vaudelet, P., Su, Z., & Chen, R. (2022). Induced Polarization as a Tool to Assess Mineral Deposits: A Review. *Minerals*, *12*(5), 571.
[13] Casulla, M. A. A., & Mizunaga, H. (2023). Characterization of potential Cu-Au mineralization using electrical resistivity and induced polarization methods: a case study in Eastern Labo, Bicol, Philippines. *Journal of Geophysics and Engineering*, *20*(2), 411-425.
[14] Zaid, H. A. H., Arifin, M. H., Kayode, J. S., Basori, M. B. I., Umor, M. R., & Hazim, S. H. (2023). Application of 2-D Electrical Resistivity Imaging, and Induced Polarization Methods for Delineating Gold Mineralization at Felda Chiku 3, Kelantan, Malaysia. *Sains Malaysiana*, *52*(1), 305-320.
[15] Yatini, Y., Zakaria, M. F., & Suyanto, I. (2026). Delineation of Sulfide Mineralization Zone Based on Geomagnetic and Induced Polarization (IP) Methods in Sangon-II, Kokap, Kulonprogo Districts, Yogyakarta. *Geofísica Internacional*, *65*(2), 2089–2099.
[16] Mohammadi, A., Abedi, M., Mirmohammadi, M., & Zarean, A. (2025). Electrical imaging of gold-bearing mineralization zones through 3D geophysical modelling. *International Journal of Mining and Geo-Engineering*, *59*(3), 237-245.
[17] Gautama, I. F. Y., Heditama, D. M., & Muttaqin, Y. A. (2018). Potensi zona urat kuarsa berdasarkan analisis geofisika dengan metode polarisasi terinduksi di daerah Olat Tanah Merah–Plampang, Kabupaten Sumbawa, Provinsi Nusa Tenggara Barat. *Buletin Sumber Daya Geologi*, 13(1), 1–14.

[18] Janghorban, G., Forooshani, S. M. A., Haroni, H. A., Sadeghisorkhani, H., & Moshtaghian, K. (2020). Magnetic and IP/RS Data Inversion for Gold Prospecting at Koh-e Lakht Epithermal Deposit, Central Iran. *3rd Conference on Geophysics for Mineral Exploration and Mining, Held at Near Surface Geoscience 2020*. (Vol. 2020, No. 1, pp. 1-5). European Association of Geoscientists & Engineers.

[19] Khoir, M. F., & Rosid, M. S. (2020). Identification of Potential Distribution of Gold Mineralization Zone of High Sulfidation Epithermal System using Time-Domain Induced Polarization (TDIP) and Magnetic Method at "n" Mountain Qrea. *IOP Conference Series: Materials Science and Engineering*, *854*(1), Article 012056.

[20] Gobashy, M. M., Eldougdoug, A., Abdelwahed, M., Abdelazeem, M., Abd El-Rahman, Y., Abdelhalim, A., & Said, S. (2023). Role of Integrated Magnetics and Geology in Tracking and Exploring Complex Structures Controlling Gold Mineralization. Example from the Fawakheir-Atalla Gold Prospects, Eastern Desert, Egypt. *Pure and Applied Geophysics*, *180*(7), 2775-2805.

[21] Bahía, M. E., Pavón Pivetta, C., Benedini, L., Costa, A., Scivetti, N., Barros, M., Gregori, D., Costa Dos Santos, A., Kostadinoff, J., & Geraldes, M. C. (2024). Gravity and magnetic geophysical surveys for exploration of low sulphidation epithermal mining project. Marifil Complex, Chon Aike Igneous Province, Argentina. *Journal of South American Earth Sciences*, *145,* 105049.

[22] Lv, H., Xu, L., Yang, B., Su, P., Xu, H., Wang, H., Yao, C., & Su, P. (2022). Mineralization Based on CSAMT and SIP Sounding Data: A Case Study on the Hadamengou Gold Deposit in Inner Mongolia. *Minerals*, *12*(11), 1404.

[23] Bitnarae Kim, Jacques Deparis, François Bretaudeau, Simon Vedrine, Jochen Kamm, Uula Autio, Cedric Patzer, Suvi Heinonen, Julien Gance, Mathieu Darnet, SEEMSDEEP working group

[24] Kim, B., Deparis, J., Bretaudeau, F., Vedrine, S., Kamm, J., Autio, U., Patzer, C., Heinonen, S., Gance, J., Darnet, M., & SEEMSDEEP Working Group. (2026). Three-dimensional geoelectrical imaging beyond 1 km depth for mineral exploration: framework of deep electrical resistivity tomography and induced polarization with advanced strategies. *Geophysical Journal International*, *244*(3), ggaf460.

[25] Loke, M. H. (2000). Electrical imaging surveys for environmental and engineering studies - A practical guide to 2-D and 3-D surveys Copyright. *Cangkat Minden Lorong*, *August 200*(1999), 61.

[26] Menke, W. (2012). *Geophysical data analysis: discrete inverse theory: MATLAB edition* (Vol. 45). Academic press.

[27] Zhao, M., Jia, M., Yang, L., Suo, K., Lu, Y., Wei, Q., & Zhang, Y. (2024). Correction methods and applications of ERT in complex terrain. *MethodsX* (Vol. 13), 103012.

[28] Yang, Y., Zhang, G., Yao, C., Deng, Z., Ren, Z., & Li, C. (2023). Application of Induced Polarization Method in Mineral Resource Exploration. *Sustainability (Switzerland)*, *15*(4), 3840

[29] Doyoro, Y. G., Gelena, S. K., & Lin, C. P. (2025). Improving subsurface structural interpretation in complex geological settings through geophysical imaging and machine learning. *Engineering Geology*, *344,* 107839.

[30] Cross, B., & Kirkland, C. L. (2021). Petrological control on chargeability with implications for induced polarization surveys. *Journal of Applied Geophysics*, *188,* 104308.

[31] Ohta, Y., Goto, T. N., Koike, K., Kashiwaya, K., Lin, W., Tadai, O., Kasaya, T., Kanamatsu, T., & Machiyama, H. (2024). Correlation between induced polarization and sulfide content of rock samples obtained from seafloor hydrothermal mounds in the Okinawa Trough, Japan. *Earth, Planets and Space*, *76*(1), 54.

[32] Chen, L., Wang, H., Sun, C., Chang, X., & Ding, W. (2025). The Application of Integrated Geochemical and Geophysical Exploration for Prospecting Potential Prediction of Copper and Gold Polymetallic Deposits in the Fudiyingzi–Bacheli Area, Heilongjiang Province. *Minerals*,

15(6), 597.
[33] Abd-Elsadek, M. K., Araffa, S. A. S., Aldeep, M., Badreldin, H., Othman, A. A. A., Mohamed, W. H., & Zaghlol, K. (2026). Geological and Geophysical Survey of Mineral Resources with an Emphasis on Gold and Associated Minerals in Atshan area,South Eastern Desert, Egypt. *Mining, Metallurgy and Exploration*, *43*(1), 463-481.
[34] Hase, J., Gurin, G., Titov, K., & Kemna, A. (2023). Conversion of Induced Polarization Data and Their Uncertainty from Time Domain to Frequency Domain Using Debye Decomposition. *Minerals*, *13*(7), 955.
[35] Porras, D., Carrasco, J., Carrasco, P., & González, P. J. (2022). Imaging extensional fault systems using deep electrical resistivity tomography: A case study of the Baza fault, Betic Cordillera, Spain. *Journal of Applied Geophysics*, *202*, 104673.
[36] Li, H., Gan, J., Gan, Y., Wang, B., Li, Y., & Jiang, W. (2023). Coupling Mechanism of the Concealed Rock Body and Metallogenic Structure of the Sarakan Gold Deposit in Laos Investigated Using Magnetic and Electrical Methods. *Minerals*, *13*(7), 912.
[37] Sono, P., Nthaba, B., Shemang, E. M., Kgosidintsi, B., & Seane, T. (2021). An integrated use of induced polarization and electrical resistivity imaging methods to delineate zones of potential gold mineralization in the Phitshane Molopo area, Southeast Botswana. *Journal of African Earth Sciences*, *174*,104060.
[38] Saeidian, B., Rajabifard, A., Atazadeh, B., & Kalantari, M. (2023). Modelling underground cadastral survey data in CityGML. *Transactions in GIS*, *27*(6), 1724-1747.
[39] Zhou, H., Li, S., Wang, Y., Lu, Y., Zhang, X., Feng, J., & Yuan, Y. (2025). Application of induced polarization gradient measurement in the exploration of the sanjiaotong gold mining area on the northern margin of the Qinghai Tibet Plateau. *Frontiers in Earth Science*, *13,* 1523261.
[40] Silver, E. A., Breen, N. A., Prasetyo, H., & Hussong, D. M. (1986). Multibeam study of the Flores Backarc Thrust Belt, Indonesia. *Journal of Geophysical Research: Solid Earth*, *91*(B3), 3489-3500.
[41] Silver, E. A., Reed, D., & McCaffrey, R. (1983). Back arc thrusting in the E Sunda arc, Indonesia: a consequence of arc-continent collision. *Journal of Geophysical Research*, *88*(B9), 7429-7448.
[42] Koulali, A., Susilo, S., McClusky, S., Meilano, I., Cummins, P., Tregoning, P., Lister, G., Efendi, J., & Syafi'I, M. A. (2016). Crustal strain partitioning and the associated earthquake hazard in the eastern Sunda-Banda Arc. *Geophysical Research Letters*, *43*(5), 1943-1949..
[43] Felix, R. P., Hubbard, J. A., Bradley, K. E., Lythgoe, K. H., Li, L., & Switzer, A. D. (2022). Tsunami hazard in Lombok and Bali, Indonesia, due to the Flores back-arc thrust. *Natural Hazards and Earth System Sciences*, *22*(5), 1665-1682.
[44] Yang, X., Singh, S. C., & Tripathi, A. (2020). Did the Flores backarc thrust rupture offshore during the 2018 Lombok earthquake sequence in Indonesia? *Geophysical Journal International*, *221*(2), 758-768.
[45] Ramdhan, M., Priyobudi, Mursityanto, A., Palgunadi, K. H., & Daryono. (2021). Analysis of M 5.3 Sumbawa, Indonesia earthquake 2020 and its aftershocks based on hypocenter relocation from BMKG seismic stations. *IOP Conference Series: Earth and Environmental Science*, (Vol. 873, No. 1, p. 012070). IOP Publishing.
[46] do Amaral, P. A. C., Borges, W. R., Toledo, C. L. B., Silva, A. M., de Godoy, H. V., & Leão Santos, M. H. (2023). Electrical Prospecting of Gold Mineralization in Exhalites of the Digo-Digo VMS Occurrence, Central Brazil. *Minerals*, *13*(12), 1483.
[47] Sierra, E. N. (2022). Ore-controlling structures and geostatistical determination of ore-shoots in shear zone hosted lode gold type deposits, El Bagre-Antioquia, Colombia. *Earth Sciences Research Journal*, *26*(1), 47-54.